Inorganic Heterocycles

A. Nordheider, T. Chivers, O. Schön, K. Karaghiosoff, K. S. Athukorala Arachchige, A. M. Z. Slawin, J. D. Woollins*

Isolatable Organophosphorus(III)–Tellurium Heterocycles

Inorganic beauty: Organophosphorus(III)–tellurium heterocycles (see figure) can be stabilized and structurally characterized by the appropriate choice of substituents in $Te_m(P^{III}R)_n$ ($m=1$; $n=2$, R = OMes* (Mes* = supermesityl or 2,4,6-tri-*tert*-butylphenyl); $n=3$, R = adamantyl (Ad); $n=4$, R = ferrocene (Fc); $m=n=3$: R = trityl (Trt), Mes*), or by the installation of a $P^{V}_2N_2$ anchor in $RP^{III}[TeP^{V}(t\text{BuN})(\mu\text{-N}t\text{Bu})]_2$ (R = Ad, *t*Bu).

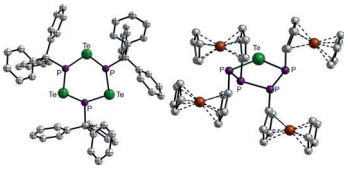

Chem. Eur. J.
DOI: **10.1002/chem.201303884**

Polychalcogenides

J. Gao, Q. Tay, P.-Z. Li, W.-W. Xiong, Y. Zhao, Z. Chen, Q. Zhang*

Surfactant–Thermal Method to Synthesize a Novel Two-Dimensional Oxochalcogenide

I can still hear you saying you would never break the chain: A new 2-dimensional (2D) oxosulfide, $(N_2H_4)_2Mn_3Sb_4S_8(\mu_3\text{-OH})_2$ (**1**), was successfully synthesized under surfactant–thermal conditions. Compound **1** has a 2D layered structure and contains a novel $[Mn_3(\mu_3\text{-OH})_2]_n$ chain along the *b*-axis. The photocatalytic activity of **1** has been demonstrated under visible-light irradiation and continuous H_2 evolution was observed.

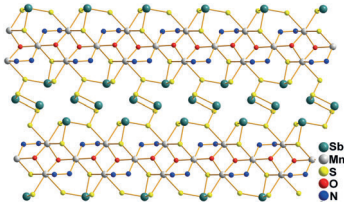

Chem. Asian J.
DOI: **10.1002/asia.201301023**

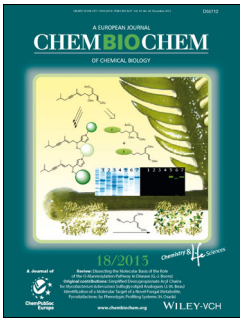

Natural Products

X. Xu, L. Liu, F. Zhang, W. Wang, J. Li, L. Guo, Y. Che,* G. Liu*

Identification of the First Diphenyl Ether Gene Cluster for Pestheic Acid Biosynthesis in Plant Endophyte *Pestalotiopsis fici*

Gene identification: The pestheic acid biosynthetic gene (*pta*) cluster was identified in *Pestalotiopsis fici*. A dihydrogeodin oxidase gene, *ptaE*, was essential for diphenyl ether formation, and *ptaM* encoded a flavin-dependent halogenase catalyzing chlorination in the biosynthesis.

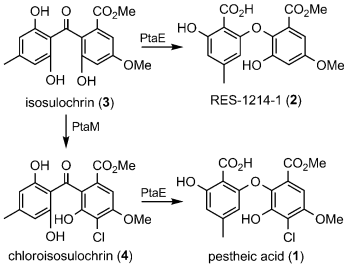

ChemBioChem
DOI: **10.1002/cbic.201300626**

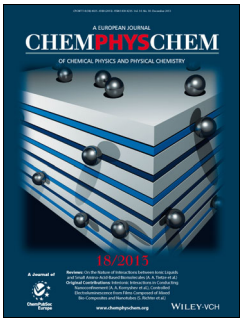

Ionic Liquids

A. A. Tietze,* F. Bordusa, R. Giernoth, D. Imhof, T. Lenzer, A. Maaß, C. Mrestani-Klaus, I. Neundorf, K. Oum, D. Reith, A. Stark

On the Nature of Interactions between Ionic Liquids and Small Amino-Acid-Based Biomolecules

Ionic liquid interactions: This Review gives a comprehensive overview of the current knowledge on the molecular basis and fundamental aspects of the interactions between amino acid-based molecules and ionic liquids, with focus on peptides and miniproteins. Technical (spectroscopy, structural biology) and theoretical (computational chemistry) prerequisites to explain the phenomena reported so far are critically assessed.

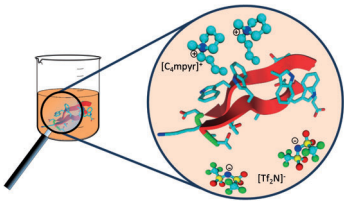

ChemPhysChem
DOI: **10.1002/cphc.201300736**

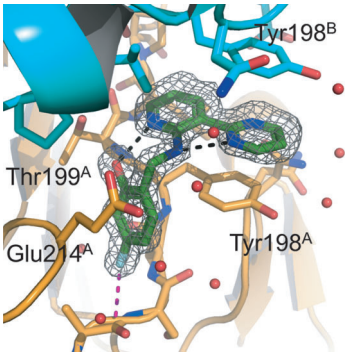

Fragment-Based Drug Design

J. Murray,* A. M. Giannetti, M. Steffek, P. Gibbons, B. R. Hearn, F. Cohen, C. Tam, C. Pozniak, B. Bravo, J. Lewcock, P. Jaishankar, C. Q. Ly, X. Zhao, Y. Tang, P. Chugha, M. R. Arkin, J. Flygare, A. R. Renslo*

Tailoring Small Molecules for an Allosteric Site on Procaspase-6

Merge ahead: A fragment-based lead discovery effort revealed the presence of a putative allosteric binding site at the dimer interface of procaspase-6. A fragment merging strategy produced nanomolar-affinity lead compounds that contact residues of the L2 loop at the dimer interface, significantly stabilizing the protein. These results suggest new avenues for controlling caspase activity and/or activation for therapeutic benefit.

ChemMedChem
DOI: **10.1002/cmdc.201300424**

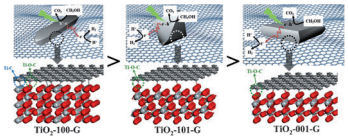

Hydrogen Production

L. Liu, Z. Liu, A. Liu, X. Gu, C. Ge, F. Gao,* L. Dong*

Engineering the TiO_2–Graphene Interface to Enhance Photocatalytic H_2 Production

Facet to facet: TiO_2–graphene nanocomposites with different TiO_2 crystal facets ({100}, {101}, and {001} facets) exposed are synthesized to investigate the effects of crystal facet on the photocatalytic properties. The interfacial charge transfer rates and electronic structures of three TiO_2–graphene nanocomposites are different, leading to their different photoactivities in photocatalytic H_2 production from methanol solution.

ChemSusChem
DOI: **10.1002/cssc.201300941**

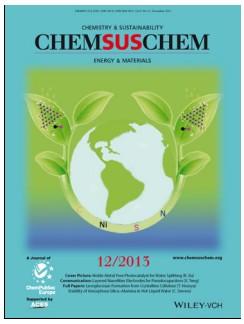

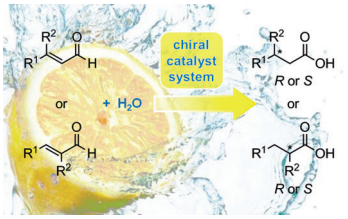

Tandem Catalysis

T. Winkler, H. Gröger,* W. Hummel*

Enantioselective Rearrangement Coupled with Water Addition: Direct Synthesis of Enantiomerically Pure Saturated Carboxylic Acids from α,β-Unsaturated Aldehydes

Making a splash with citral: The direct one-pot transformation of α,β-unsaturated aldehydes to saturated carboxylic acids using only water proceeds with perfect atom economy. This tandem process involves two redox biotransformations without need of additional external co-substrates for cofactor regeneration. With, for example, citral as prochiral α,β-unsaturated aldehyde, transformation to (*S*)-citronellic acid proceeds with >99% conversion and >99% *ee*.

ChemCatChem
DOI: **10.1002/cctc.201300764**

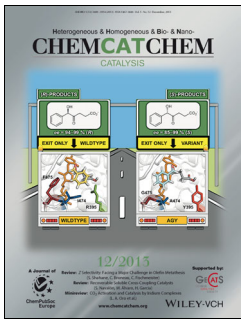

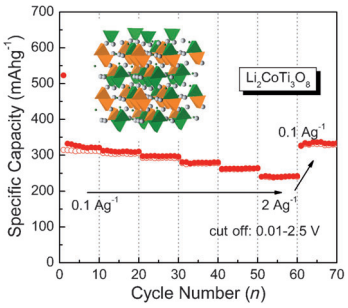

Electrochemistry

J. Wang, H. Zhao,* Y. Shen, Z. Du, X. Chen, Q. Xia

Structure, Stoichiometry, and Electrochemical Performance of $Li_2CoTi_3O_8$ as an Anode Material for Lithium-Ion Batteries

Less is more: The synthesized nonstoichiometric $Li_2CoTi_{2.682}O_8$ exhibits high specific capacity (320 mA h g^{-1}) and excellent rate capability (160 mA h g^{-1} at 20 C; 1 C corresponds to 300 mA g^{-1}; see figure). The nonstoichiometric material with Ti-site deficiency provides a high theoretical specific capacity and a decreased bandgap for electron conduction, which ensures good electronic conductivity and therefore an excellent rate capability.

ChemPlusChem
DOI: **10.1002/cplu.201300235**

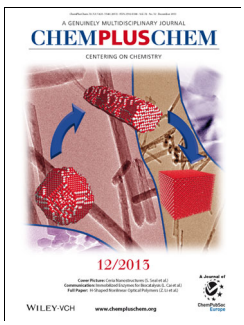

Electrocatalysis

E. Fabbri,* R. Mohamed, P. Levecque, O. Conrad, R. Kötz, T. J. Schmidt

$Ba_{0.5}Sr_{0.5}Co_{0.8}Fe_{0.2}O_{3-\delta}$ Perovskite Activity towards the Oxygen Reduction Reaction in Alkaline Media

Perovskite catalysts: Cyclic voltammograms in Ar- and O_2-saturated KOH reveal that the onset for the oxygen reduction reaction (ORR) occurs at potentials below ~0.77 V_{RHE}. Rotating ring-disk electrode measurements and Koutecky–Levich analysis prove that for $Ba_{0.5}Sr_{0.5}Co_{0.8}Fe_{0.2}O_{3-\delta}$, the ORR does not fully proceed via a four-electron process, leading to the parallel formation of OH^- and HO_2^- (see picture).

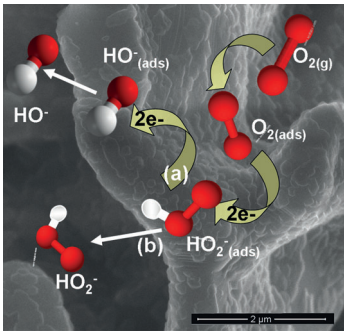

ChemElectroChem
DOI: **10.1002/celc.201300157**

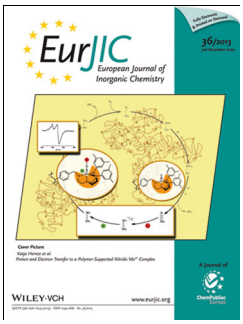

Sulfonate Complexes

P. Thuéry*

Molecular and Polymeric Uranyl and Thorium Complexes with Sulfonate-Containing Ligands

Four sulfonate-containing ligands, some having additional carboxylate groups, were used to synthesize uranyl and thorium(IV) cation complexes, which crystallize as 0D, 1D or 3D assemblies. Monodentate or bridging bidentate sulfonate coordination is observed, and the results show, as phosphonates, that sulfonates have great potential for the synthesis of actinide–organic coordination polymers and frameworks.

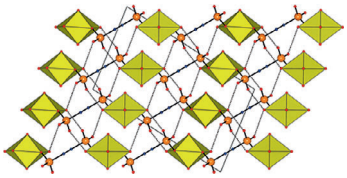

Eur. J. Inorg. Chem.
DOI: **10.1002/ejic.201301258**

Total Synthesis

S. Müller, F. Sasse, M. E. Maier*

Synthesis of Pladienolide B and Its 7-Epimer with Insights into the Role of the Allylic Acetate

Pladienolide B (**1**) and 7-*epi*-pladienolide B (**42**) were both prepared by the reduction of an enone precursor, that is, through a chelation-controlled reduction of an acyclic enone (for **1**) or the reduction of a macrocyclic enone precursor (for **42**). The correct configuration of the allylic acetate group at C-7 is crucial. Although synthetic **1** was highly cytotoxic, epimer **42** was completely inactive.

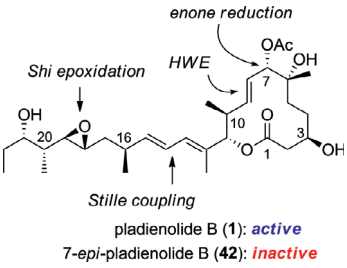

Eur. J. Org. Chem.
DOI: **10.1002/ejoc.201301468**

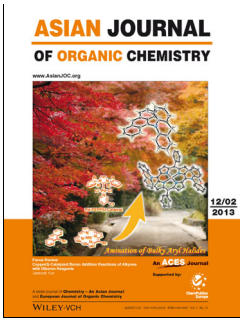

Macrocyclic Dyads

S. Pla, L. Martín-Gomis, K. Ohkubo, S. Fukuzumi,*
F. Fernández-Lázaro, Á. Sastre-Santos*

Macrocyclic Dyads Based on C_{60} and Perylenediimides Connected by Click Chemistry

Fuller surprises: Two perylenediimide (PDI)-[60]fullerene macrocyclic dyads connected through 1,2,3-triazole units have been synthesized and characterized. A small interaction between the C_{60} and PDI units in the ground state was detected by UV/vis and electrochemical measurements in both PDI-C_{60} cyclic systems. The occurrence of photoinduced energy-transfer processes between PDI and C_{60} were confirmed by time-resolved emission and transient absorption techniques.

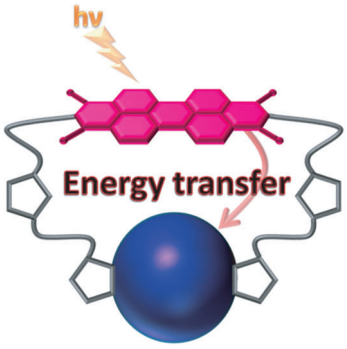

Asian J. Org. Chem.
DOI: **10.1002/ajoc.201300235**